UNIVERSITY OF NIS FACULTY OF MECHANICAL ENGINEERING

THE TENTH INTERNATIONAL CONFERENCE
TRANSPORT AND LOGISTICS

https://doi.org/10.46793/TIL2025.013D

til 2025

APPLICATION OF COMPUTATIONAL AND EXPERIMENTAL METHODS IN THE ANALYSIS AND DESIGN OF MODERN VERTICAL-ROPE TRANSPORT SYSTEMS

Radomir ĐOKIĆ[1], Jovan VLADIĆ[1], Tanasije JOJIĆ[1]

[1)] *Department of Mechanization and Design Engineering, Faculty of Technical Sciences, University of Novi Sad*

ORCID iDs: Radomir ĐOKIĆ https://orcid.org/0000-0002-1578-0543
Jovan VLADIĆ https://orcid.org/0000-0003-1518-1935
Tanasije JOJIĆ https://orcid.org/0000-0002-2174-3394

Abstract

The analysis of the dynamic behavior of vertical-rope systems is a complex task and represents an essential step in the design process and in establishing the conditions for the safe and efficient operation of such systems. The development of machines and equipment for vertical transport with specific characteristics, such as modern elevators and mine hoisting systems operating at great lifting heights and high velocities (exceeding 20 m/s), has necessitated the formulation of new computational procedures for analyzing their dynamic behavior. Because of its exceptional properties, steel wire rope is one of the most widely used structural elements in engineering. The complex construction of steel wire rope, which provides these properties, also affects its mechanical characteristics. Since the stiffness of steel wire rope can be more than twice lower than that of other elements used in the construction and manufacturing of components for vertical transport machinery, its influence on the dynamic behavior is significantly greater, making the analysis of such systems considerably more complex. This paper presents an analysis of the application of analytical-numerical and experimental procedures in the design of systems related to specific transport machines in which steel wire rope is the dominant element (elevators and mine hoisting systems). Using state-of-the-art computational-experimental methods, the paper presents specific results concerning the dynamic behavior of machines with a vertical rope as the load-bearing element.

Keywords: *vertical-rope transport systems, experimental methods, numerical methods.*

1 INTRODUCTION

A steel wire rope, due to its exceptional properties (high flexibility and the ability to transmit large tensile loads), is one of the most widely used structural elements in engineering. Its complex construction, which provides these properties, significantly affects its mechanical behavior. As a result, deformations - especially for long lengths - are considerably larger than those observed in "standard" structural load-bearing elements. Consequently, its influence on the dynamic behavior of such systems is substantially greater, and the analysis becomes much more complex [1]. In addition to its role as a load-bearing element in transport machinery, steel wire rope is also used as a functional element for power and motion transmission in systems with drive sheaves and drums.

The development of machines and equipment for vertical transport with specific characteristics, such as modern elevators and mine hoisting systems operating at great lifting heights and high velocities (up to 20 m/s), has created the need for new computational procedures to analyze their dynamic behavior [2]. Existing calculation methods, based on models of oscillating elastic elements of constant length, cannot account for the effects of high velocities and variable boundary conditions occurring at the points where the rope enters and leaves the drive sheave [3-5]. During high-speed hoisting, changes in stiffness caused by the reduction of the rope's free length can lead to unstable motion or resonant phenomena with unpredictable consequences. Furthermore, defining realistic parameters of dynamic models (stiffness, damping, motion resistances, etc.) represents a key challenge in analyzing the dynamic behavior of such systems [6].

The fundamental "tools" in the design process are established computational-experimental procedures [7]. These procedures are used for verification, shaping, and dimensioning of machine structural components. This body of knowledge, methods, techniques, and procedures is commonly referred to as engineering analysis, which relies on both theoretical and experimental approaches. Theory and experiment are complementary methods, and today the experimental approach is most often used to validate the theoretical model.

The demands of industry and modern society have driven the development and application of vertical-transport machinery with specific characteristics - primarily elevators and mine hoisting systems operating at great heights and lifting velocities in high-rise buildings and underground mining facilities. Vertical-transport devices today are neither a luxury nor a matter of prestige; they have become essential components of modern structures that continuously push the limits of construction in terms of height, making them indispensable and necessary for the efficient transport of people and goods between floors of skyscrapers.

1.1. Application of Steel Wire Ropes in Elevators and Mine Hoisting Systems

Hoisting ropes used in elevators must exhibit good fatigue resistance, high breaking strength, and low elongation. Fig. 1, for example, shows the recommendations for selecting elevator ropes depending on the lifting height, as provided by the rope manufacturer "*Brugg Group AG*".

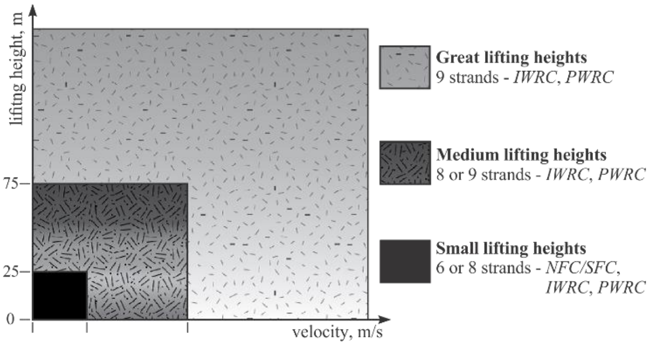

Fig. 1 *Recommendations for elevator rope selection*

For elevators with low and medium lifting heights, single-layer *Seale* construction ropes with 6 or 8 strands are most commonly used. Eight-strand steel ropes are "rounder" than six-strand ropes, which allows for a greater number of contact points between the rope and the sheave groove, resulting in more favorable contact pressures. In addition, eight-strand ropes contain wires of smaller diameter compared to six-strand ropes, which is advantageous in terms of bending performance, but less favorable in applications with pronounced wear on the contact surfaces of sheaves and pulleys. This indicates that the optimal rope selection depends on the specific operating conditions. In recent years, for machine-room-less (MRL) elevators, in addition to the above types, single-layer *Warrington* construction ropes with 6 strands and an independent wire rope core (IWRC) have been widely used. They are suitable for small-diameter sheaves and applications where space savings are required.

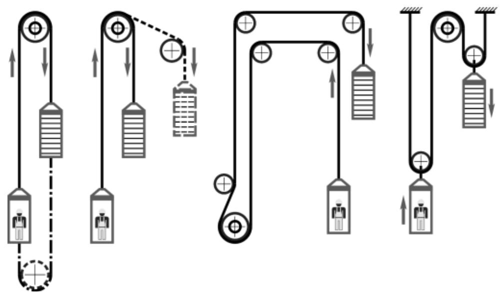

Fig. 2 *Elevator schematics*

For elevators with medium lifting heights, multi-layer *Seale* construction ropes with 9 strands in the outer layer are also used. They possess high breaking strength and excellent flexibility, making them suitable for elevators with a larger number of diverting sheaves (multiple rope reavings), as shown in Fig. 2. These ropes typically feature a fiber core (NFC/SFC) or a metal core with parallel-lay strands (PWRC). Some of the ropes previously mentioned for low and medium lifting heights may, in certain cases, also be applied in systems with large lifting heights. However, for high lifting velocities (up to 20 m/s), which are common in modern elevators, the use of high-performance steel wire ropes is essential. The most commonly used ropes in such applications are multi-layer *Seale* construction ropes with 9 strands in the outer layer. Compared to 8-strand ropes, they provide a rounder cross-sectional profile, greater flexibility, and higher breaking strength. The core is either an independent wire rope core (IWRC) or a metal core with parallel-lay strands (PWRC). In addition to *Seale* constructions, *Warrington* construction ropes are also encountered in high-rise elevator installations. They are a good choice for sheaves with wide undercut grooves, and the thicker outer-layer wires make them suitable for applications with pronounced wear.

In mine hoisting systems (Fig. 3), Seale construction ropes, either single-layer or multi-layer (with regular or reverse lay), are most commonly used. The core is an independent wire rope core (IWRC), either without coating or with thermoplastic sheathing (EPIWRC). These ropes must exhibit high flexibility and wear resistance. Due to the great depths of mine shafts, and regardless of the guiding of the cage and the counterweight, it is desirable for the ropes to be non-rotating.

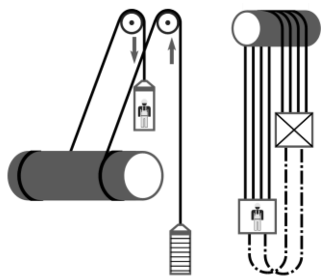

Fig. 3 *Mine hoisting system schematics*

Multi-layer ropes are most commonly used as compensation ropes. They must exhibit good non-rotating properties, and, as with hoisting ropes, the core is an independent wire rope core, either without coating (IWRC) or with a thermoplastic covering (EPIWRC).

2. MECHANICAL CHARACTERISTICS OF STEEL WIRE ROPES

Based on the analysis, the mathematical description of a steel wire rope in service is highly complex, primarily due to its intricate construction. For analyzing systems in which a steel wire rope functions either as a structural or functional element, it is necessary to know a number of its characteristics, such as breaking strength, flexibility, modulus of elasticity, fatigue strength, resistance to wear and corrosion, structural stability, and others. In this paper, the most important characteristics required to describe the behavior of transport machinery with so-called "vertical" ropes (elevators and hoisting systems) under load will be defined.

2.1. Breaking Strength of a Steel Wire Rope

Since a rope consists of twisted wires and strands, its breaking strength depends on the sum of the breaking forces of the individual wires and the type of lay, that is, the rope construction. As an illustration, Fig. 4 shows a stress-strain diagram of a wire with a diameter of δ = 1.06 mm after the so-called patenting process, i.e., a combination of deformation and heat treatment, by which the tensile strength of the wires may be R_m = 1370, 1570, 1770, 1960, 2160, or 2450 MPa.

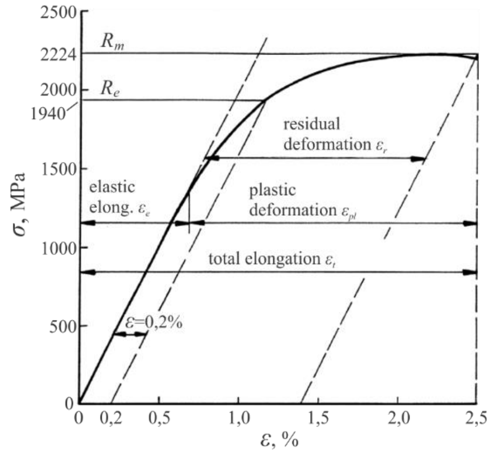

***Fig. 4** Stress-strain diagram of a wire with a diameter of δ = 1.06 mm [8]*

According to rope standards, the following values are defined:

Calculated breaking force: $F_r = R_m \cdot A$

where:

$A = \sum_i \frac{\delta_i^2 \cdot \pi}{4} = f \cdot A' = f \cdot \frac{d^2 \cdot \pi}{4}$ - metallic cross-sectional area of the rope

$A' = \frac{d^2 \cdot \pi}{4}$ - nominal cross-sectional area of the rope

d - rope diameter

δ - wire diameter

i - number of wires

$f = \frac{A}{A'}$ - fill factor, with typical values of 0.3–0.5 for ropes with a fiber core, 0.5–0.6 for ropes with a steel core, and approximately 0.7–0.9 for coiled rope.

Minimum breaking force: $F_{\min} = k \cdot F_r$

where: k=0.7÷0.9 - lay factor (depending on rope construction).

Measured total breaking force: $F_i = \sum_j F_{ij}$

where: F_{ij}- measured breaking force of an individual wire.

Maximum working force: $S_{\max} = \frac{F_r}{\upsilon}$

where: υ safety factor.

2.2. Stiffness and Modulus of Elasticity

Stiffness is defined by the expression [1] and [9]:

$$c = \frac{E \cdot A}{L - l(t)} \tag{1}$$

In addition to depending on changes in the free rope length, stiffness also depends on the modulus of elasticity, which is most often treated as a constant value in dynamic analyses. However, due to the complex construction of a steel wire rope (consisting of wires, strands, and a core), its variation with respect to stress level and loading characteristics (loading–unloading) cannot be neglected. Because of the twisting of wires and strands, the stress-strain diagram is no longer a straight line. Fig. 5 shows the curves for the base wire material, the wire after patenting, as well as for a strand and for the rope. It can be seen that the initial part of the strand curve is no longer linear, because transverse contraction of the helically laid wires occurs until they are fully tightened, after which the strand, or rotation-laid rope, begins to behave as a unified element. This nonlinearity is even more pronounced in ropes composed of multiple strands. In addition to the nonlinearities in the initial portion of the diagram, twisted ropes and strand-based ropes exhibit a significant reduction in the slope of the curves, i.e., in the modulus of elasticity, as well as lower peak stress values.

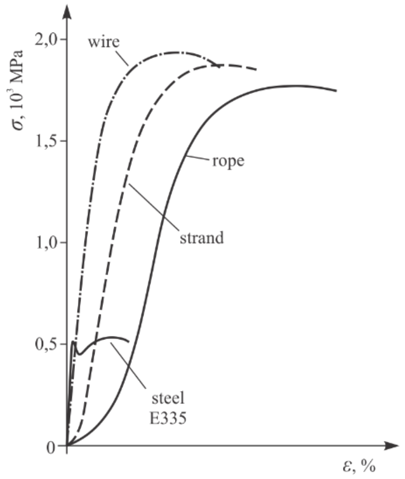

***Fig. 5** Stress-strain relationships for the steel, wire, strand, and rope*

According to [8], two types of elastic modulus are distinguished: the tangent modulus of elasticity (E_t) and the average modulus of elasticity between two stress levels (E_s), as shown in Fig. 6 The tangent modulus of elasticity represents the theoretical slope of the tangent to the σ–ε curve at the current stress value (σ_z). A continuous variation in the modulus of elasticity is evident, and it must also be taken into account whether the curve corresponds to loading (E_{to}) or unloading (E_{tr}) of the rope, which is unfavorable for practical use, particularly in dynamic analysis. Linearization of the modulus of elasticity is performed by determining its average value between two operating stresses, E_s (σ_d, σ_g). Compared to the variable tangent modulus of elasticity, defining an average modulus value becomes more significant. If the lower stress is σ_d = 0, the average modulus of elasticity becomes dependent on the maximum operating stress value, i.e., E_s (0, σ_z).

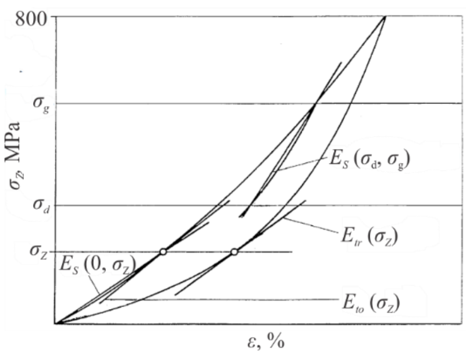

Fig. 6 *Tangent and average modulus of elasticit ofa rope [8]*

Calculating the rope's modulus of elasticity based on the modulus of elasticity of the wires and the lay angles of the wires in the strand and the strands in the rope provides only approximate values, because the actual modulus depends, besides the parameters listed above, on the stress level, the core material, service time (number of load cycles), lay type and direction, type of wire contact, and other factors. Therefore, defining a general expression for the modulus of elasticity of stranded ropes is practically impossible without experimental data. Fig. 7 shows the experimental results presented in [8] for a steel wire rope with a natural-fiber core. A clear difference can be observed between the results for the first loading cycle (new rope) and after ten loading and unloading cycles (Fig. 7a). Fig. 7b shows the influence of stress level during loading and unloading, where pronounced hysteresis effects at different stress levels are evident.

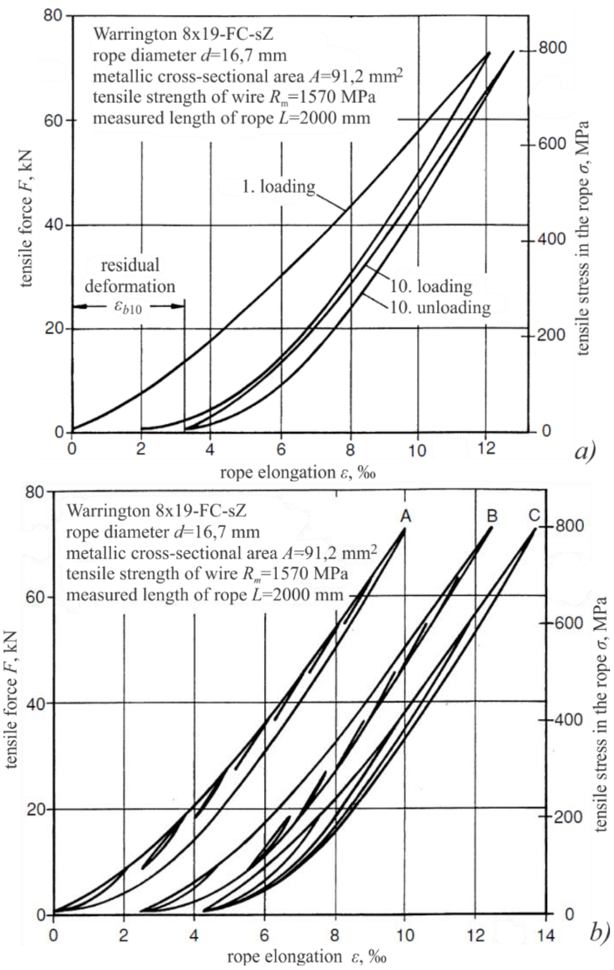

Fig. 7 *Stress-strain diagrams for ropes with a fiber core: a) in the case of a new rope and after 10 load cycles, b) after the tenth loading cycle for different stress levels [8]*

The change in tensile stress for ropes with a steel core is shown in Fig. 8. More details on this analysis and the results of this experiment are provided in [8].

The value of the tangent elastic modulus according to [8] can be determined from the expression:

$$E_t(\sigma_z) = C_0 + \frac{C_1}{\sigma_z + A} + \sum_{i=2}^{n} C_i \cdot x_i \tag{2}$$

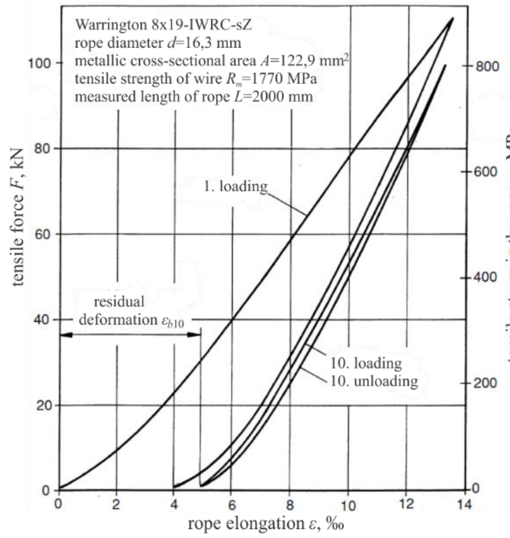

Fig. 8 *Change in tensile stress for ropes with a steel core, in the case of a new rope and after 10 load cycles [8]*

Based on experiments with different types of ropes with strands and on processing the measurement results using linear regression analysis, the values of the coefficients C_0, C_1, C_i and A were defined and are given in tabular form in [8].

The average values of the elastic modulus are defined by the expression:

$$E_S(\sigma_d, \sigma_g) = \frac{\sigma_g - \sigma_d}{\dfrac{\sigma_g - \sigma_d}{B_{d,g}} - \dfrac{C_d}{B_{d,g}^2} \cdot \ln \dfrac{\sigma_g + A_d + C_d / B_{d,g}}{\sigma_d + A_d + C_d / B_{d,g}}} \tag{3}$$

In the case where the lower stress value is $\sigma_d = 0$ the above expression takes the form:

$$E_S(\sigma_z) = \frac{\sigma_z}{\dfrac{\sigma_z}{B_0} - \dfrac{C_0}{B_0^2} \cdot \ln\left(1 + \dfrac{\sigma_z}{A_0 + C_0 / B_0}\right)} \tag{4}$$

where: $E_S(\sigma_z) = E_S(0, \sigma_z)$

Considering that the test results were obtained under laboratory conditions with a relatively slow change of loading and unloading, the application of such results is questionable when dealing with dynamic processes. Therefore, appropriate elastic modulus values for ropes in service can be obtained through direct measurements under real operating conditions. Some values of the elastic modulus of ropes in operation based on [10] are given in Table 1.

Table 1 Elastic modulus of ropes in service [10]

Type of rope	E_s, 10^5 MPa
round wire	2,0
spiral rope, closed	1,45…1,72
spiral rope, open	1,25…1,45
strand rope, multi-layer	1,00…1,25
strand rope with metal core	1,00…1,25
strand rope with fiber core	0,70…1,00

2.3. Damping

In many practical systems, oscillation energy is gradually transformed into heat or sound, the effect mostly known as damping. Although the quantity of such energy is relatively small, it is important to dedicate some attention to damping to predict the oscillatory system's response, such as the elevator systems considered in this paper.

Damping at ropes used in vertical transport systems is complex, and it happens because of the rope's inner friction (viscous and hysteretic damping), Coulomb's friction on guide rails and damping due to the airflow around the cabin (cage) in the elevator shaft [11] and [12]. The friction on the elevator guide rails creates the damping force (Coulomb's friction), which is constant in its magnitude, but it is of the opposite direction compared to the motion of the oscillating load. Since this type of elevator requires special attention to be paid to the guiding accuracy and reducing the guide rails friction, in the example with centrical cabin load, the friction forces can be neglected in relation to the total load. Nevertheless, the influence can be of importance for cabin oscillation analyses [13]. A typical diagram of an oscillator with Coulomb's friction is presented in Fig. 9a. The declining of amplitudes, as opposed to inner friction oscillation, is linear in its nature [12] and [14].

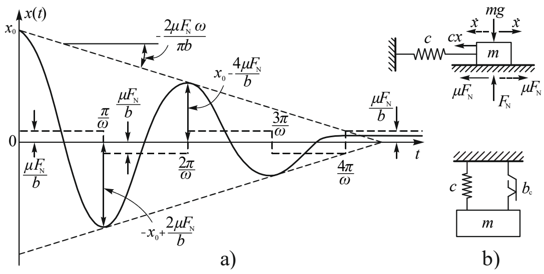

Fig. 9 *An oscillating system with Coulomb's friction: a) motion with the load, b) a model with Coulomb's damping*

As it was explained in [11], the total force of Coulomb's friction on guide rails is:

$$F_{\mathrm{c}} = n_{\mathrm{v}} \cdot n_{\mathrm{t}} \cdot \mu \cdot F_{\mathrm{N}} \tag{5}$$

For the most part, the literature presents the inner friction in the rope as viscous friction, like in homogenous bodies. Nevertheless, while the rope is being deformed, the energy dissipation also appears due to the friction between wires and strands, which slide against one another during the deformation process. This creates the hysteresis loop (Fig. 10a). The effect causes the damping known as hysteretic or structural damping. The loss of energy per unit of material volume in one loading and unloading cycle is equal to the area closed by the hysteresis loop. Experiments have confirmed that the energy loss per cycle is approximately proportional to the square of the oscillating amplitude. A model with hysteretic damping is presented in Fig. 10b. Similarly to the above, the rope's inner friction (b_r) is a combination of viscous and hysteretic damping, Fig. 10c.

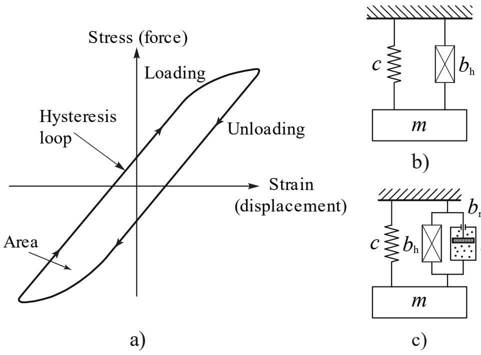

Fig. 10 *Hysteretic damping: a) hysteresis loop, b) a model with hysteretic damping, c) and an equivalent model with internal rope damping [12]*

The total damping of the considered system is an overall influence of the damping due to the rope's internal friction and the damping caused by the friction in guide rails, so it can be represented by the parallel connections in the oscillator model, Fig. 11b.

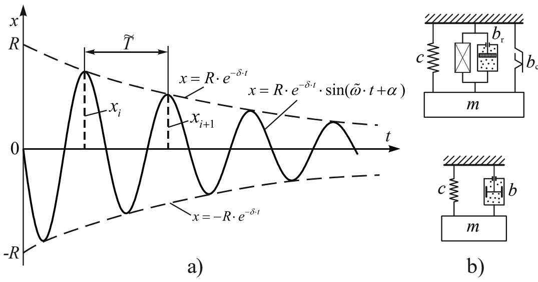

Fig. 11 *Oscillating system with viscous integral damping: a) damped oscillations b) a lifting system model*

By measuring the amplitudes and oscillating periods of free damping oscillations (changes in cage acceleration), the damping coefficient (δ) can be determined via a logarithmic decrement, and based on this, a resistance force coefficient (b):

$$D = \ln \frac{x_i}{x_{i+1}} = \frac{1}{n} \ln \frac{x_i}{x_{i+n}} = \delta \cdot \tilde{T} \ \rightarrow \ \delta = \frac{D}{\tilde{T}} \tag{6}$$

$$b = 2 \cdot \delta \cdot M_{\mathrm{e}} \tag{7}$$

Determining the stiffness coefficient (c) and elasticity modulus (E) of hoist ropes can be performed with the measured oscillation parameters (oscillating period, oscillating amplitudes, etc.):

$$c = M_{\mathrm{e}} \cdot \omega^2 \tag{8}$$

$$E = \frac{c \cdot L}{A} \tag{9}$$

3. CHARACTERISTICS OF VERTICAL LIFTING MACHINES

In addition to the well-known systems used in traction elevators (traction sheaves), the most commonly applied hoisting systems in mining hoist installations with a drive drum and traction transmission (Köepe system) are schematically shown in Fig. 12.

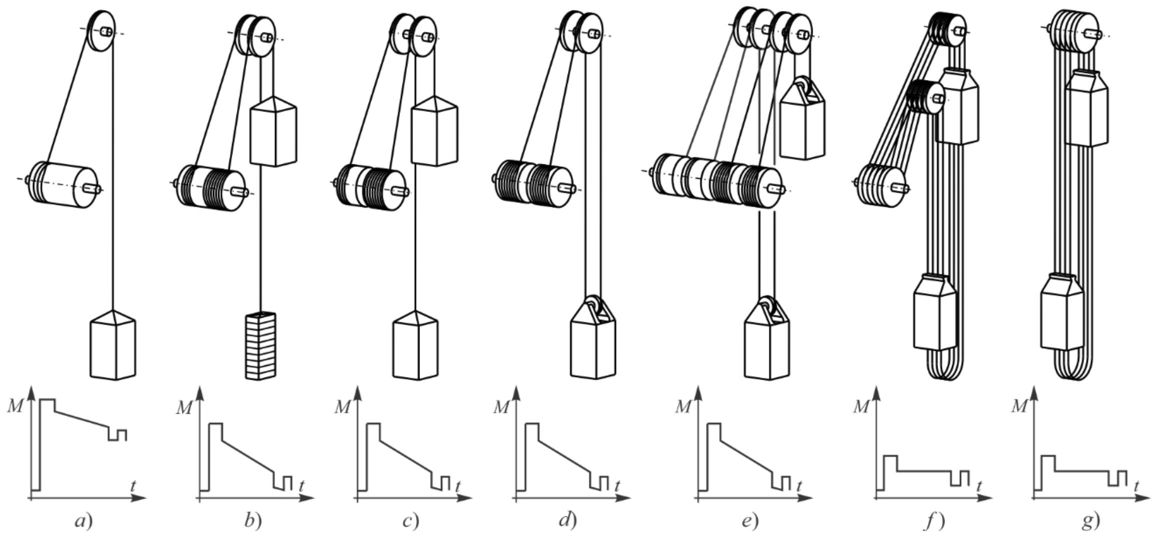

Fig. 12 *Hoisting systems with a drum (a-e) and Köepe systems (f, g)*

In drum-type hoisting systems, the carrying ropes are wound and stored on the drum. A single-drum hoisting system (Figs. 12a, b) has limited application due to the large loads involved and the required drum length. However, a two-drum system (Fig. 12c) allows lifting two separate “loads” within the same hoisting (mine) shaft - for example, one “load” may be the cage and the other a counterweight, as in standard elevator installations, or, as is often the case in mines, both “loads” may be “active,” with one cage being raised while the other is lowered.
The drums are installed in a machine room located laterally with respect to the shaft, and the ropes run from the drums over deflection sheaves down the shaft to the cage. A multi-rope hoisting system (Figs. 12d, e) used in mine hoists is essentially a variation of the two-drum system. It is used for heavier loads and in relatively deep shafts.
Traction hoisting systems (Köepe systems) are most commonly used in European mines. The drive is installed either above the shaft (Fig. 12g) or laterally (Fig. 12f), in which case deflection sheaves are placed above the cage and the counterweight. The main advantages of this system are reduced motor power (and consequently reduced required torque), simpler use of multiple wire ropes, and the possibility of locating the traction sheave directly above the shaft. However, due to limitations on contact pressure (1.75 MPa) and slippage ($S_1 / S_2 \leq 1.4$) between the ropes and the traction sheave, these advantages diminish, so in practice both systems are used almost equally.

3.1. Dynamic Models of Traction-Sheave Hoisting Systems

For determining dynamic loads in the case of vertical hoisting using a traction sheave, the dynamic models shown in Fig. 13 are most commonly adopted. In these models, m_1 - is the reduced mass of the drive part, m_2 - is the mass of the cage and the payload, and P - is the driving force. Fig. 13a illustrates a rope model appropriate for hoisting systems in which the lifting height and lifting velocity are relatively small, which allows the rope to be considered an inelastic flexible element. This figure represents the so-called rigid-kinematic model of an elevator.

The forming of a dynamic model for vertical-transport machines can be separated into three parts. First, the rope model as the load-bearing element can be defined. Figs. 13b, 13c, and 13d show two-degree-of-freedom dynamic models, which are very frequently used in elevator analyses.

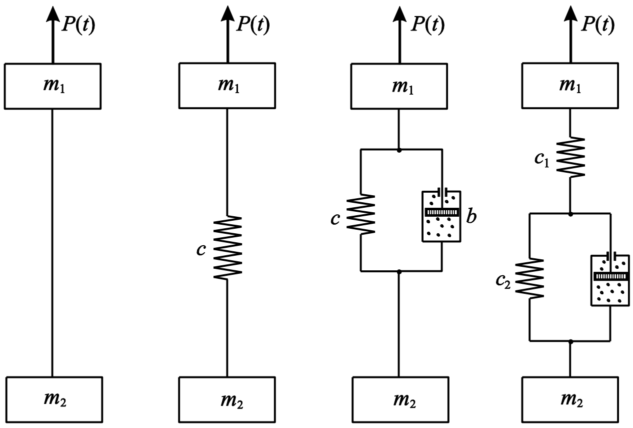

Fig. 13 *Dynamic models of the load-bearing element: a) inelastic element, b) Hooke model, c) Kelvin model, d) the standard model*

The model with the load-bearing element represented as a rod (“heavy” rope) of constant length. For greater hoisting heights, the influence of the weight of the steel rope must be taken into account. This can be approximated as a single-degree-of-freedom oscillatory system with a “heavy” spring, as treated in general literature. However, the problem can be modelled more accurately as a system with an infinite number of degrees of freedom (longitudinal oscillations of a rod) with appropriate boundary conditions.
The forming of the differential equations of motion for a rope of constant length can be performed by considering one side only (the side on which the cage is located). This is justified because the rope length remains constant; in essence, longitudinal oscillations of a rod of length L are considered [15]. The consideration will be carried out according to Fig. 14.

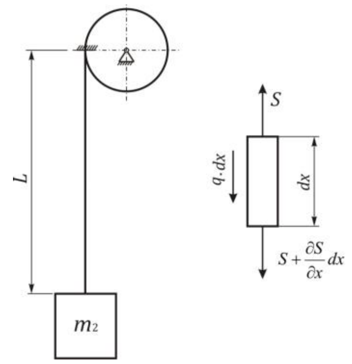

***Fig. 14** Oscillation of a rope of constant length*

Based on D'Alembert's principle, considering the equilibrium of an infinitesimal rope segment, the following can be written:

$$\frac{q}{g}\cdot\frac{\partial^2 u}{\partial t^2} = E\cdot A\cdot\frac{\partial^2}{\partial x^2}\left(u + b\cdot\frac{\partial u}{\partial t}\right) + q \tag{10}$$

If oscillations around the equilibrium position (the position of static equilibrium) are considered, where $v(x,t)$ denotes the displacement from the equilibrium position, and $u(x,0)=u_{st}$ is the rope elongation caused by its own weight, the differential equation of motion for a rope of constant length takes the form [16]:

$$\frac{\partial^2 v}{\partial t^2} = \frac{g\cdot E\cdot A}{q}\cdot\frac{\partial^2}{\partial x^2}\left(v + b\cdot\frac{\partial v}{\partial t}\right) \tag{11}$$

A solution to Eq. (11) can be sought in the form of a product of two functions, each dependent on a single variable only:

$$v(x,t) = X(x)\cdot T(t) \tag{12}$$

If expression (12) is differentiated twice and substituted into Eq. (11), two ordinary differential equations are obtained:

$$\begin{aligned}&\ddot{T} + b\cdot k^2\cdot c^2\cdot\dot{T} + k^2\cdot c^2\cdot T = 0\\ &X'' + k^2\cdot X = 0\end{aligned} \tag{13}$$

where: $c^2 = \dfrac{g\cdot E\cdot A}{q}$ - the wave propagation velocity.

The solution of the second equation has the form:

$$X(x) = A_1\cdot\cos(k\cdot x) + A_2\cdot\sin(k\cdot x) \tag{14}$$

The constants A_1 and A_2 are determined from the boundary conditions [16]

a) for x=0, based on Fig. 14, the extension is equal to zero, i.e., $u(0,t)=0$, so the first boundary condition is $v(0,t)=0$.

b) for $x=L$, the second boundary condition is: $\dfrac{Q}{q}\cdot\left(\dfrac{\partial^2 v}{\partial t^2}\right)_{x=L} = -E\cdot A\cdot\dfrac{\partial}{\partial x}\left(v + b\cdot\dfrac{\partial v}{\partial t}\right)_{x=L}$

The complete solution of the system of ordinary differential equations (13), and thus of Eq. (11), is given in [16]. Here, only the part of the solution procedure related to determining the frequency equation of rope oscillations with a load at the lower end, in the case when the driving sheave is stationary, will be presented.

By using the second boundary condition and substituting it into Eqs. (13) and (12), after rearranging, one obtains [16]:

$$k\cdot L\cdot \mathrm{tg}(k\cdot L) = \frac{q\cdot L}{Q} \tag{15}$$

By introducing the notations $\beta=k\cdot L$ and $\alpha=(q\cdot L)/Q$, the frequency equation of rope oscillations with a load at the lower end, in the case of a stationary driving sheave, becomes:

$$\beta\cdot\tan\beta = \alpha \tag{16}$$

For different ratios of the rope weight and the load, the above equation can be solved numerically or graphically. The equation has infinitely many roots, hence the number of natural circular frequencies is infinite.

For characteristic values of β (from 0 to $7\pi/2$, depending on the number of equation roots and on the ratio of the rope and load masses, i.e., the value of α), the corresponding mode shapes of rope oscillations are defined as:

$$X_i(x) = A_2\cdot\sin(k\cdot x) = A_2\cdot\sin\left(\beta_i\cdot\frac{x}{L}\right) \tag{17}$$

For large hoisting heights and small cage capacities, when the values of α are significant, the values of β:

$$\beta = \frac{2n-1}{2}\cdot\pi \tag{18}$$

where: n=1, 2, 3, …

The model with a "heavy" rope of variable length. For hoisting machines with large lifting heights and high travel velocities, the previously mentioned models are not adequate, due to the fact that during hoisting, not only does the weight of the free rope segment change significantly, but the fundamental parameter of dynamic models - the stiffness EA/l, also varies considerably [17,18]. The relevant dynamic model for describing the dynamic behavior of systems with a driving sheave is shown in Fig. 15.

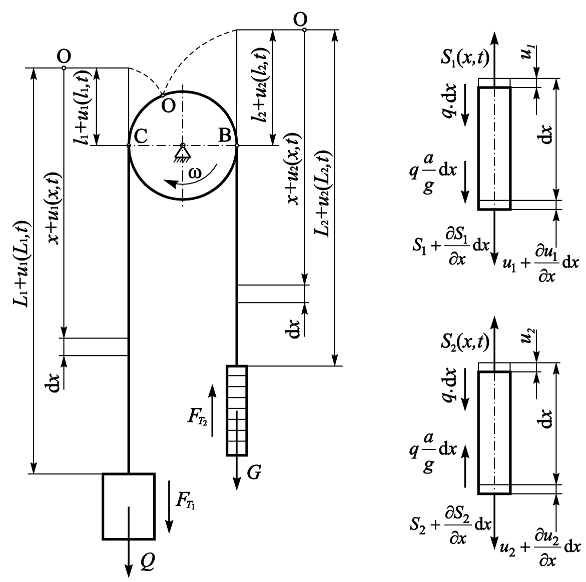

***Fig. 15** Dynamic model of a machine with a vertical rope [19], [11]*

The model shown in Fig. 15 enables a comprehensive analysis of the dynamic behavior of an elevator, incorporating the influence of the varying length of the free rope leg on its stiffness $c=E\cdot A/l$ (parametric oscillations). Such a model must be applied for high-speed and express elevators, as well as for mine hoisting installations, when analyzing the dynamic behavior and motion stability of the system.

Based on the equilibrium of the elementary segments of the ascending and descending rope branches, and the moments acting on the driving sheave (Fig. 15), the dynamic behavior is defined using a system of three partial differential equations in the form [19]:

$$\frac{q}{g}\cdot\frac{\partial^2 u_1(x,t)}{\partial t^2}=E\cdot A\cdot\frac{\partial^2}{\partial x^2}\cdot\left[u_1(x,t)+b\cdot\frac{\partial u_1(x,t)}{\partial t}\right]+q\cdot\left(1\pm\frac{a}{g}\right) \quad (19)$$

$$\frac{q}{g}\cdot\frac{\partial^2 u_2(x,t)}{\partial t^2}=E\cdot A\cdot\frac{\partial^2}{\partial x^2}\cdot\left[u_2(x,t)+b\cdot\frac{\partial u_2(x,t)}{\partial t}\right]+q\cdot\left(1\pm\frac{a}{g}\right) \quad (20)$$

$$\begin{aligned}M_m=\frac{R}{i\cdot\eta}\cdot E\cdot A\cdot\frac{\partial}{\partial x}\cdot\Big\{&u_1(l_1,t)-u_2(l_2,t)+\\&+\frac{\partial}{\partial t}\left[u_1(l_1,t)-u_2(l_2,t)\right]-J_r\cdot\frac{a\cdot i_R}{\eta}\Big\}\end{aligned} \quad (21)$$

where:
u_1, u_2 - elastic deformation of the rope,
E - modulus of elasticity,
A - cross-sectional area of the rope,
a - acceleration of the drive mechanism,
M_m- motor driving torque,
i_R - gear transmission ratio,
η - drive efficiency,
J_r - rotational inertia of the rotating masses reduced to the sheave shaft,
R - radius of the sheave.

By representing the rope using the Kelvin model, the following can be written:

$$S(x,t)=E\cdot A\cdot\frac{\partial}{\partial x}\cdot\left[u(x,t)+b\cdot\frac{\partial u(x,t)}{\partial t}\right] \quad (22)$$

where: b - coefficient accounting for internal friction (damping parameter).

To solve the given system of equations, it is necessary to define the boundary conditions at the points where the rope enters and leaves the drive sheave, as well as at the points where the rope ends are attached to the car and the counterweight.

If it is assumed that there is no slipping of the rope on the drive sheave (i.e., the traction conditions are satisfied), the boundary condition at the point where the rope enters the drive sheave, Fig. 16, can be written in the following form [19]:

$$u_1(l_1,t)=\int_0^t\frac{\partial u_1(l_1,t)}{\partial x}\left(\frac{dl_1}{dt}\right)\cdot dt \quad (23)$$

where:
l_1 - the length of rope wound on the sheave,
$\frac{dl_1}{dt}$ - the rope winding (hoisting) velocity.

If elastic slip of the rope occurs on the drive sheave, the boundary condition is:

$$u_1(l_1,t)=\int_0^t\frac{\partial u_1(l_1,t)}{\partial x}\left(\frac{dl_1}{dt}-\frac{d}{dt}(\Delta l_1)\right)\cdot dt+\Delta l_1\cdot\frac{\partial u_1(l_1,t)}{\partial x} \quad (24)$$

where: $\frac{d}{dt}(\Delta l_1)$ - is the elastic slip velocity.

The boundary condition at the rope attachment point on the cabin is:

$$\begin{aligned}Q=E\cdot A\cdot\frac{\partial}{\partial x}&\left(u_1(L_1,t)+b\cdot\frac{\partial u_1(L_1,t)}{\partial t}\right)+\\&+\left(\frac{Q}{g}\cdot\frac{\partial^2 u_1(L_1,t)}{\partial t^2}-a\right)\end{aligned} \quad (25)$$

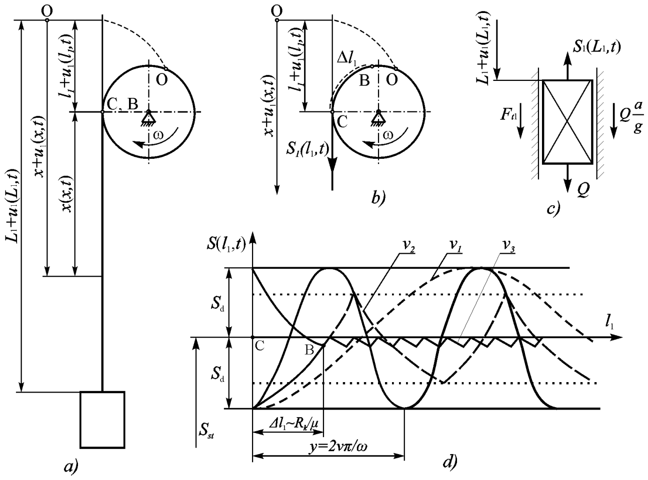

Fig. 16 *Boundary conditions: a) on the sheave without slip, b) on the sheave with slip, c) on the cabin [19]*

At high hoisting velocities, the rate of change of the rope tension over the sheave wrap angle is smaller than the friction force, so the rope tension remains in the portion of the angle corresponding to relative rest, as it was before reaching the sheave.

Due to the variable tension in the descending rope branch, parametric oscillations may also occur. Accordingly, the ascending and descending rope branches can be considered separately in cases where kinematic conditions are imposed on the drive sheave (i.e., the loads do not affect the drive mechanism).

4. ANALYSIS AND APPLICATION OF ANALYTICAL-NUMERICAL METHODS FOR SOLVING MATHEMATICAL MODELS

The analysis of vertical-transport systems and machines involves the formulation of mathematical models in the form of systems of differential and algebraic equations. A large number of analytical-numerical methods and procedures for solving such mathematical models are available in the literature. Fig. 17 shows a diagram [20] illustrating the workflow and approaches for solving real-world problems using mathematical models.

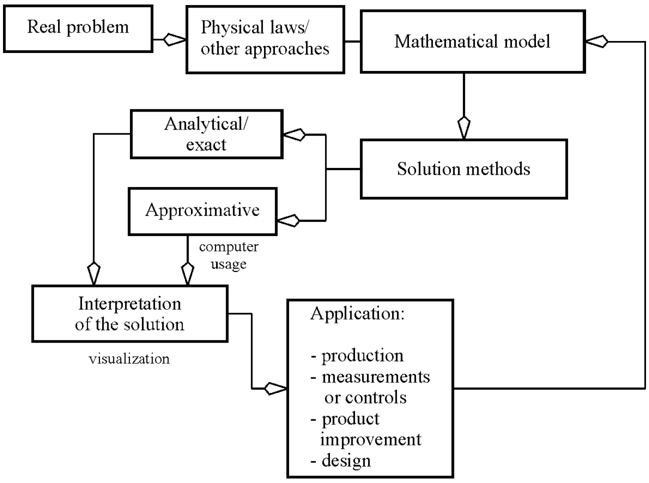

Fig. 17 *Flowchart for solving mathematical models [20]*

4.1. Significant Methods for Solving the Mathematical Model of a System with a Vertical Rope

There is a large number of analytical methods for solving differential equations [1], but these methods are limited to special cases. These procedures yield solutions in a general form, and by applying initial conditions, unique solutions can be obtained. However, for many problems (often related to the mathematical models of most technical systems), it is not possible to apply analytical methods, making it necessary to resort to numerical approximation. A numerical solution is desirable even in cases where a closed-form solution exists, but is very complicated. For example, the numerical solution of a differential equation is often given in the form of a table, so that the analytical expression of the function remains unknown. The practical applicability of analytical methods (especially in the context of transport machines with vertical ropes) is very limited.

For solving ordinary differential equations in the field of hoisting machinery, the Euler polygonal method is most commonly used as the basis of many numerical methods, as well as the second-order Runge-Kutta method, which are well-known in the literature. Therefore, they will not be discussed in detail here.

4.2. Methods for Solving Mathematical Models with Partial Differential Equations

In this brief explanation, the focus will be on second-order partial differential equations used to describe the behavior of systems with a "vertical" rope [21]. As is well known from the general literature, the general form of a second-order partial differential equation is:

$$\begin{aligned} &a(x,y)\frac{\partial^2 u}{\partial x^2}+b(x,y)\frac{\partial^2 u}{\partial x \partial y}+c(x,y)\frac{\partial^2 u}{\partial y^2}+ \\ &+d(x,y)\frac{\partial u}{\partial x}+e(x,y)\frac{\partial u}{\partial y}+f(x,y)u=g(x,y) \end{aligned} \tag{26}$$

Based on the value of the so-called discriminant:

$$D(x,y)=b^2-4ac \tag{27}$$

partial differential equations are classified as parabolic (D=0), hyperbolic (D>0), or elliptic (D<0).

The problem of longitudinal oscillations in load-bearing ropes of vertical transport machines belongs to the group of hyperbolic-type equations (D>0). For solving such mathematical models, the finite difference method and the method of separation of variables are most commonly used.

1. *Finite difference methods*

The finite difference method for numerical solving of partial differential equations comprises:

- Discretization of the area (domain) of the independent variables,
- Approximation of partial derivatives with finite differences,
- Solving the resulting system of algebraic equations.

That means that the inside points of the area (mesh) satisfy the differential equation, and the points on the boundary of the area (domain) satisfy the boundary conditions.

The basic idea behind the finite difference method is in the replacement of derivatives of the considered function with their approximate values. In the realization of the idea we introduce points, i.e. mesh of nodes (hence the name – mesh method), where we look for the solution.

To consider the specific cases, such as elevators and exploitation facilities in mines, we are going to take a look at the one-dimensional partial differential equation of the hyperbolic type of the second order.

$$\frac{\partial^2 u}{\partial t^2}-a(x,t)\frac{\partial^2 u}{\partial x^2}=f(x,t) \tag{28}$$

where $a(x,t)>0$ for every x and $t>0$.

In the boundary area for the variable coordinate x (for instance a change in the length of the free rope end with the elevators where the total length is L) we define the boundary conditions, such as Fig. 18:

$$\begin{cases} u(0,t)=g_1(t) \\ u(L,t)=g_2(t) \end{cases} \quad \text{for } t>0 \tag{29}$$

And also the initial conditions, Fig. 18:

$$\begin{aligned} &u(x,0)=u_0(x),\ x\in\{0,L\} \\ &\left.\frac{\partial u}{\partial t}\right|_{(x,t=0)}=v_0(x),\ x\in\{0,L\} \end{aligned} \tag{30}$$

In which the second condition is known as the so-called Cauchy's condition.

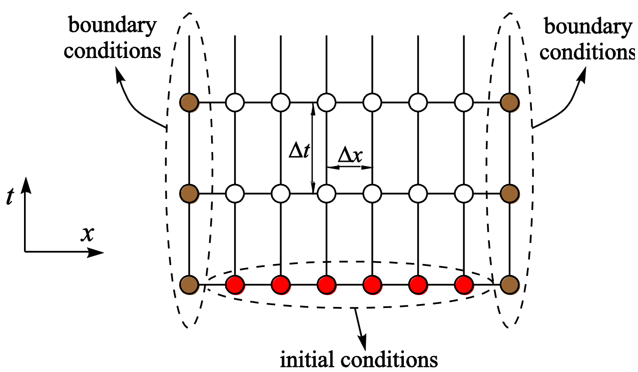

Fig. 18 *Mesh of nodes with boundary and initial conditions*

If we introduce the $a(x,t)=c^2$, in which c represents the positive constant, then the general (analytical) solution for (28) is given in the form of:

$$u(x,t)=\frac{f(x+ct)+f(x-ct)}{2}+\frac{1}{2c}\int_{x-ct}^{x+ct} v_0(x)dx \tag{31}$$

For the sake of a more comprehensible explanation we will introduce signs N and K, representing the number of points in the spatial coordinate x and the number of points (divisions) per time coordinate t. For that reason the function $u(x,t)$ changes into the form of u_n^k. By introducing the extra signs:

$$x_n = n\cdot\frac{L}{N},\ t_k = k\cdot\frac{T}{K} \tag{32}$$

where $0\le n\le N$ and $0\le k\le K$
L - total spatial coordinate (length),
T - total (final) integration time,
And then the boundary and initial conditions become:

$$\begin{cases} u_0^k = g_1(t_k) \\ u_N^k = g_2(t_k) \end{cases} \quad 0\le k\le K \tag{33}$$

$$\begin{cases} u_n^0 = u_0(x_n) \\ \left.\dfrac{\partial u}{\partial t}\right|_{n,0} = v_0(x_n) \end{cases} \quad 0\le n\le N \tag{34}$$

By using the central difference theory and by replacing the suitable derivatives in time and place coordinate x, it can be written that:

$$\begin{aligned} \frac{\partial^2 u}{\partial t^2} &= \frac{u_n^{k+1}-2u_n^k+u_n^{k-1}}{\Delta t^2} \\ \frac{\partial^2 u}{\partial x^2} &= \frac{1}{2}\left(\frac{u_{n+1}^{k+1}-2u_n^{k+1}+u_{n-1}^{k+1}}{\Delta x^2}+\frac{u_{n+1}^{k-1}-2u_n^{k-1}+u_{n-1}^{k-1}}{\Delta x^2}\right) \end{aligned} \tag{35}$$

where: $\Delta t = T/K$ and $\Delta x = L/N$.

By introducing the sign (abbreviation) $\lambda=\dfrac{\Delta t^2}{\Delta x^2}$, we get the system for (N-1) equations as a replacement for the partial differential equation in the area from (k+1) points per time. In order to solve the system, we have to know the field at the (k+1) point.

$$-\frac{1}{2}\lambda a_n^{k+1}u_{n-1}^{k+1}+\left(1+\lambda a_n^{k+1}\right)u_n^{k+1}-\frac{1}{2}\lambda a_{n+1}^{k+1}u_{n+1}^{k+1}=\frac{1}{2}\Delta t^2\left(f_n^{k+1}+f_n^{k-1}\right)+2u_n^k-\left[\frac{\lambda}{2}a_n^{k-1}u_{n-1}^{k-1}-\left(1-\lambda a_n^{k-1}\right)u_n^{k-1}+\frac{\lambda}{2}a_n^{k-1}u_{n+1}^{k-1}\right] \tag{36}$$

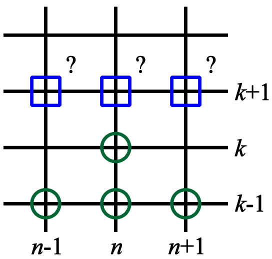

Fig. 19 *Illustration of the time-space mesh with a wave equation*

According to (36), in order to reach the solution, we also have to know the field (values) in (k-1) points. This is enabled by the initial conditions (34). Using the development in Taylor's order per t we get:

$$u_n^k = u_n^{k-1}+\left.\frac{\partial u}{\partial t}\right|_{k-1}\Delta t+\frac{1}{2}\left.\frac{\partial^2 u}{\partial t^2}\right|_{k-1}\Delta t^2 \tag{37}$$

All that is needed is to determine the u_n^1, in which we write the following according to (28):

$$\begin{aligned} u_n^1 &= u_n^0+v_n^0\Delta t+\frac{1}{2}f_n^0\Delta t^2+ \\ &+\frac{1}{2}\lambda a_n^0\left(u_{n+1}^0-2u_n^0+u_{n-1}^0\right)\quad \text{for } \left(1\le n\le N-1\right) \end{aligned} \tag{38}$$

By taking into consideration a special case (homogenous differential equation where $f(x,t)=0$ and using the already mentioned positive constant $a(x,t)=c^2$, we get a simple system of algebra equations:

$$\begin{aligned} &\left(1+\alpha\right)u_n^{k+1}-\frac{1}{2}\alpha u_{n+1}^{k+1}-\frac{1}{2}\alpha u_{n-1}^{k+1}= \\ &=2u_n^k+\frac{1}{2}\alpha u_{n+1}^{k-1}-\left(1+\alpha\right)u_n^{k-1}+\frac{1}{2}\alpha u_{n-1}^{k-1} \end{aligned} \tag{39}$$

where: $\alpha=c^2\dfrac{\Delta t^2}{\Delta x^2}$.

Equation (39) represents an excellent form and basis for solving such problems in a numerical way in contemporary software tools, such as MATLAB, Mathcad, Mathematica and so on.

2. *Fourier's Method of Separation of Variables*

Like the finite difference method, the method of separation of variables will be presented through a simple case - the homogeneous one-dimensional wave equation, i.e., a special form of a hyperbolic-type partial differential equation, given by expression (28). Its special form (the wave equation) is:

$$\frac{\partial^2 u}{\partial t^2}-c^2\frac{\partial^2 u}{\partial x^2}=0 \tag{40}$$

with the initial and boundary conditions (34), (33):

$$\begin{cases} u(x,0)=u_0(x) \\ \dfrac{\partial u(x,0)}{\partial t}=v_0(x) \end{cases} \quad 0\le x\le L \tag{41}$$

$$\begin{cases} u(0,t)=g_1(t) \\ u(L,t)=g_2(t) \end{cases} \quad 0\le t\le T \tag{42}$$

For the special form - the wave equation (40), the boundary conditions are zero (both ends fixed), i.e., $g_1(t)=g_2(t)=0$.

The method of separation of variables gives the function $u(x,t)$ in the form:

$$u(x,t) = X(x) \cdot T(t) \tag{43}$$

where X and T are functions of x and t, respectively.
By substituting expressions (43) and (40) and differentiating twice with respect to x and t, one obtains:

$$X(x)\ddot{T}(t) - c^2 T(t) X''(x) = 0 \tag{44}$$

or, by separating variables:

$$\frac{\ddot{T}(t)}{c^2 T(t)} = \frac{X''(x)}{X(x)} \tag{45}$$

Since the left-hand side is a function of t only, and the right-hand side is a function of x only, this equality can hold only if both functions are equal to a constant, e.g. $-k^2$. This leads to two ordinary differential equations:

$$\ddot{T} + k^2 \cdot c^2 \cdot T = 0 \tag{46}$$

$$X'' + k^2 \cdot X = 0 \tag{47}$$

The solutions of these two equations are of the form:
$T = A\cos(kct) + B\sin(kct)$
$X = C\cos(kx) + D\sin(kt)$
Hence, the particular solution of equation (40) is:

$$u = \left[A\cos(kct) + B\sin(kct)\right] \cdot \left[C\cos(kx) + D\sin(kt)\right] \tag{48}$$

The constants A, B, C and D are determined from the initial (41) and boundary (42) conditions, depending on the specific problem. For particular cases and equations of motion, some complete solutions and derivations are provided in [15]. In systems with vertical hoisting of loads, i.e., systems described by differential equations of load oscillations on load-bearing ropes, the proper definition of initial and boundary conditions is of crucial importance, as it directly affects the solution of equation (48).
The method of separation of variables primarily belongs to analytical methods; however, with the development of programming languages and application software for numerical analysis, it has become highly suitable for practical use.

5. APPLICATION OF EXPERIMENTAL METHODS IN DETERMINING THE DYNAMIC BEHAVIOR OF MACHINES WITH VERTICAL ROPES

This paper presents the application and significance of experimental analysis in the design of transport machines [9]. Specifically, measurements performed on a mine hoisting machine with a load capacity of 22 t, a maximum designed hoisting velocity of 16 m/s, and a designed hoisting height of 523 m in the first phase and 763 m in the second phase of ore extraction are taken as an example. A schematic representation of the machine and the measurement locations are shown in Fig. 20. The hoisting shaft has a circular cross-section with a diameter of 10 m. The transmission of force to the load-bearing elements (ropes) is achieved via friction (Köepe system) from a grooved drum. Other detailed technical characteristics of the hoisting machine can be found in [1].

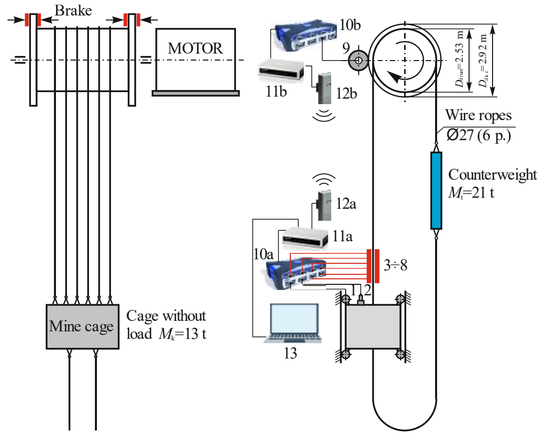

Fig. 20 *Schematic layout of the measuring places*

The experiment was done according to the principle of summary data acquisition via a wireless data transfer, by using the NanoStation loco NS2L antennas (pos. 12a and 12b, Fig. 20). This way, a complete synchronization of the collected data on the cage roof and machine room was achieved. The drum number of revolutions was measured with an AINS 41 incremental encoder (pos. 9, Fig. 20). It was set on the adaptive carrier with a 127 mm diameter measuring wheel, which was directly leaned onto the rim of the brake disc, Fig. 21a. The encoder measuring signal was led to the amplifier (pos. 10b, Fig. 20), and then via a LAN switch (pos.11b, Fig 20) and the antenna (pos. 12b) wirelessly connected to the other radio antenna positioned on the cage (pos. 12a). The measuring signal was stored in a common computer file (pos. 13) placed on the cage. It was done via another LAN switch (pos. 11a).

a) *b)*

Fig. 21 *Measuring places: a) the incremental encoder connected with the measuring wheel positioned on the rim of the brake disc, b) the optical sensor (number of revolutions sensor) positioned on the cage*

The lifting and lowering velocity of the cage was measured via a roller guide, whose change in the number of revolutions was registered with an optical sensor (pos. 1, Fig. 20), positioned on a small magnet table, Fig. 21b. The change in the cage's acceleration during the measuring process was registered by an HBM B12 accelerometer (pos. 2), set on the cage. The force changes in the hoist ropes were monitored by measuring the deformation of the connecting tools (pos. 3÷8, Fig. 20). The deformations were measured on each connecting tool (out of 6 in total), by using the HBM LY41-6/120 strain gauges.
All measuring signals were led to the other eight-channel measuring amplifier (pos. 10a, Fig. 20) and they were

recorded on the computer (pos. 13) via an LAN switch (pos. 11a).
This paper will present some of the measurement results relevant for determining the dynamic parameters of vertical rope machines. Experiment results and determination of the dynamic model parameters are shown in four characteristic motion cases (lifting and lowering) of the cage, with and without load. A significantly higher number of measurements was completed for different cases (different positions for starting and stopping the cage motion etc.) and the results are presented in [1]. Here, the results of lowering and lifting of an empty cage and a loaded cage (traction machine) are presented. According to those, the system oscillation parameters are defined. The characteristics of experimental cases are as follows:

I) Lowering an empty cage from position +104 m to position +56 m (48 m). The action of stopping the cage was performed by suddenly switching off the driving electromotor (at a high velocity, Fig. 22a).

II) Lifting of an empty cage from position +56 m to a position +199 m (143 m). Stopping the cage was done just like in the case above, with the sudden switching off the power to the driving electromotor - at a high velocity, Fig. 22b.

III) Lifting a loaded cage (the traction machine for wagons - mass ~9.35 t) from position a -71 m, to position +52 m (123 m). Stopping the cage was done at a low velocity, Fig. 22c.

IV) Lowering the loaded cage (the traction machine for wagons - mass ~9.35 t) from position +52 m to -71 m (123 m). Stopping the cage was done at a low velocity, Fig. 22d.

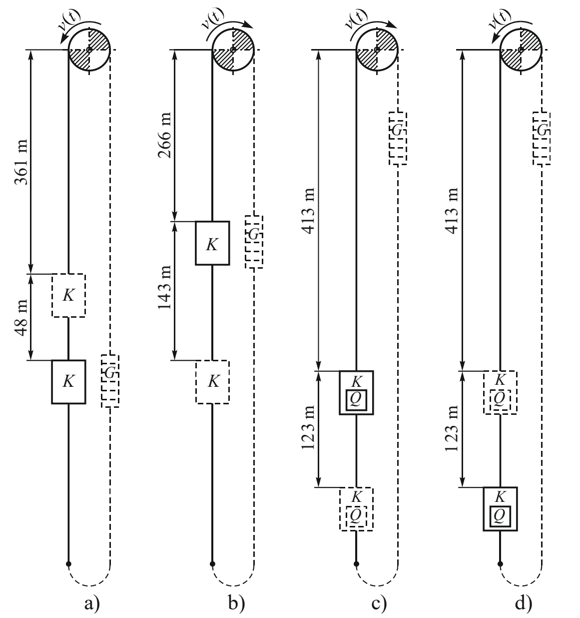

Fig. 22 *Mine elevator parameters that are relevant for the analysis: a) lowering an empty cage, b) lifting of an empty cage, c) lifting a loaded cage d) lowering the loaded cage*

The results of the conducted experimental research can be seen in the following figures, which are showing the changes in the winding velocities of hoist ropes that were wound onto the drum; cage acceleration and changes in the forces in the hoist ropes on the place the elements for connecting the ropes to the cage. The results are valid for all four chosen examples of motion. The diagram shows the character of the changes of the said parameters. It shows the cage oscillation amplitudes that occur after stopping the driving machine. This part of the diagram (after stopping the driving machine) is used to set the mechanical characteristics of steel ropes (harmonic oscillations).

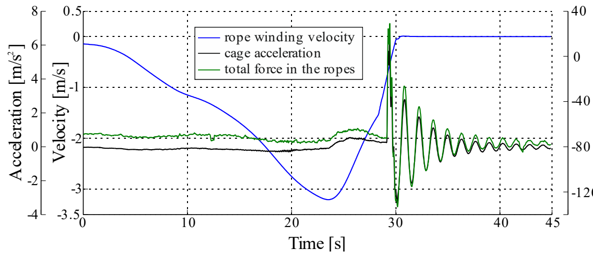

Fig. 23 *Diagram with the results obtained during lowering an empty cage and sudden stopping, at a "high" velocity (I motion case)*

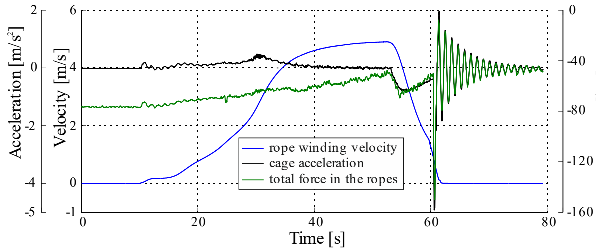

Fig. 24 *Diagram with the results obtained during lifting the empty cage and sudden stopping, at a "high" velocity (II motion case)*

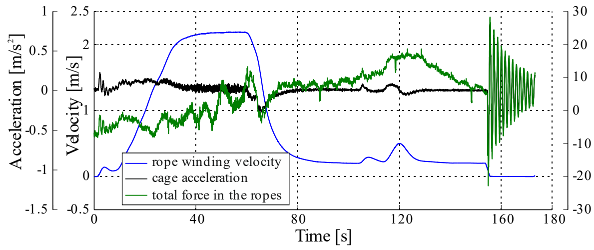

Fig. 25 *Diagram with the results obtained during the loaded cage lifting process (III motion case)*

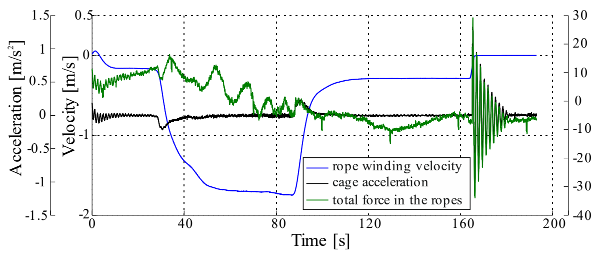

Fig. 26 *Diagram with the results obtained during loaded cage lowering process (IV motion case)*

5.1. Method of Determining Dynamic Parameters Based on Experiments

The stiffness and damping parameters can be determined, and the elasticity modulus as mechanical characteristics of a steel rope can be indirectly determined too, by using the above diagrams and determining the oscillation period, i.e. the frequency and logarithm decrement of the damping. Based on the diagram in Fig. 23÷26 and the expression 6÷9, mechanical characteristics of steel ropes are defined, as shown in Table 2. Upon analyzing the measured results, it can be concluded that the data for elasticity modulus are in agreement with the data from the literature [8]. The higher values of elasticity modulus for loaded cabins are seen as a consequence of the rope that was constructed by putting the lays of wires in strands, and strands into a rope. This confirms the validity of the applied procedure, enabling us to define the real (exploitation) values in mine elevators. The damping coefficient values, for which there is no significant comparative data, are not constant in size, but appear to be different in the analyzed experiments. Regarding the limitations in conducting the experiments in working conditions, it was concluded that the experiment should be prepared in a laboratory setting in the future.

Table 2 Values obtained by measuring and parameters of hoist ropes

	L [m]	M_e [kg]	δ [s^{-1}]	ω [rad/s]	c [N/m]	b [Ns/m]	E [MPa]	δ/ω
I (Fig. 13a) ↓	409	18 797	0.33	4.67	409 163	12 222	98 440	0.070
II (Fig. 13b) ↑	266	20 525	0.21	5.69	663 329	8718	103 792	0.037
III (Fig. 13c) ↑	413	28 099	0.09	4.26	510 803	5161	124 095	0.022
IV (Fig. 13d) ↓	536	26 613	0.18	3.88	401 206	9639	126 498	0.047

6. CONCLUSION

The dynamic analysis and scientific approach shown in this paper are of special importance taking into account the nature of the systems - they are meant for lifting (lowering) people and load to great heights (depths) at velocities up to 20 m/s. The complexity of the dynamic analysis can also be seen in the fact that these are oscillating processes with variable parameters and boundary conditions at the incoming/outgoing points of the steel rope and the driving pulley. Furthermore, the stiffness and elasticity modulus of steel ropes are not constant in magnitude, but rather change depending on the changes in cage position, as well as construction, stress, and rope exploitation time.

The paper presents an experimental method that can be used to determine dynamic parameters such as stiffness, elasticity modulus, and damping in exploited elevator steel ropes. Certain elasticity modulus values that are presented in the chapter 5 reveal the noticeable dependence on the load, i.e. rope stress. In addition, the damping coefficient in ropes is not a constant size, but it depends on the position of a cage. It can be deduced that ropes experience a combination of viscous damping and hysteretic damping, which should be further investigated in these systems.

For driving mechanisms used for vertical load lifting (elevators and cranes), it is necessary to provide adequate conditions for the correct dynamic analysis of their parts' behavior and especially for the rope as the basic element, already in the design phase. Due to a significant influence of rope free length changes, due to its slipping over the driving pulley and for the reason of its mechanical characteristics, it is impossible to apply a classical dynamic model of longitudinal oscillations for homogenous stick of a constant length, especially by the elevators with large velocities and large lifting heights (express and mine elevators).

The system of partial differential equations of the hyperbolic type is possible to be solved by using the numerical methods, but only in the cases after stopping (braking) the driving mechanism. In that case we trust the stiffness suits the current values of the rope's free length as a constant size with the suitable boundary conditions.

REFERENCES

1. Vladić, J., Đokić, R., Jovanović, M., 2019, *Steel wire rope and computational-experimental procedures for the analysis of specific transport machines*, University of Novi Sad, Faculty of Technical Sciences, Novi Sad
2. Li, C., Hua, C., Qin, J., Zhu, Z., 2019, *Research on the Dynamic Characteristics of High-Speed Elevator System*, Advances in Engineering Research, 181, pp. 105-109, DOI: 10.2991/ice2me-19.2019.23.
3. Guo, Y., Zhang, D., Chen, K., Feng, C., Ge, S., 2018, *Longitudinal dynamic characteristics of steel wire rope in a friction hoisting system and its coupling effect with friction transmission*, Tribology International, 119, pp. 731-743, DOI: 10.1016/j.triboint.2017.12.014.
4. Watanabe, S., Okawa, T., 2018, *Vertical vibration of elevator compensating sheave due to brake activation of traction machine*, Journal of Physics: Conference Series, 1048(012012)
5. Đokić, R., Vladić, J., Gajić, A., Živanić, D., 2014, *Numerical analysis of elevator ropes vibration with time varyng length*, Proc. of the Eighth International Conference HEAVY MACHINERY - HM 2014, Zlatibor, Serbia, pp. A.119-124.
6. Herrera, I., Su, H., Kaczmarczyk, S., 2010, *Investigation into the damping and stiffness characteristics of an elevator car system*, Applied Mechanics and Materials,24-25, pp. 77-82. DOI: 10.4028/ www.scientific.net/AMM.24-25.77.
7. Arrasate, X., Kaczmarczyk, S., Almandoz, G., Abete, J. M., 2014, *The modelling, simulation and experimental testing of the dynamic responses of an elevator system*, Mechanical Systems and Signal Processing, 42(1-2), pp. 258-282, DOI: 10.1016/j.ymssp.2013.05.021.
8. Feyrer, K., 2007, *Wire Ropes*, University of Stuttgart, Germany.
9. Đokić, R., Vladić, J., Kljajin, M., Jovanović, V., Marković, G., Karakašić, M., 2021, *Dynamic Modeling, Experimental Identification and Computer Simulations of Non-Stationary Vibration in High-Speed Elevators*, Strojniški vestnik - Journal of Mechanical Engineering, 67(6), pp. 287-301, doi:10.5545/sv-jme.2020.7179.

10. Scheffler, M., 1994, *Grundlagen der Fördertechnik – Elemente und Triebwerke*, Friedr. Vieweg & Sohn., Braunschweig/Wiesbaden.
11. Vladić, J., Jovanović, M., Đokić, R., Kljajin, M., Karakašić, M., 2015, *Theoretical and experimental analysis of elevator dynamic characteristics*, Tehnički vjesnik / Technical Gazette, 22(4), pp. 1011-1020, DOI: 10.17559/TV-20150107175453.
12. Rao, S. S., 2011, *Mechanical vibrations*, Prentice Hall, Upper Saddle River.
13. Zhang, X., Li, H., Meng, G., 2008, *Effect of Friction on the Slide Guide in an Elevator System*, Journal of Physics: Conference Series, 96(012074).
14. Goroshko, O. A., 2007, *Evolution of the dynamic theory of hoist ropes*, International Applied Mechanics, 43(1), pp. 64-67, DOI: 10.1007/s10778-007-0007-9.
15. Vujanović, B., 1995, Theory of oscillations (in Serbian), University of Novi Sad.
16. Vladić, J., 1982, *Contribution to the determination of the safety degree against slipping of a dynamically loaded rope in the power transmission system by a driving pulley*, Master's thesis, University of Novi Sad, Faculty of Technical Sciences, Novi Sad.
17. Zhang, Q., Yang, Y., Hou, T., Zhang, R., 2019, *Dynamic analysis of high-speed traction elevator and traction car–rope time-varying system*, Noise & Vibration Worldwide, 50(2), pp. 37-45, DOI: 10.1177/0957456519827929.
18. Bao, J., Zhang, P., Zhu, C., 2012, *Modeling of Rope Longitudinal Vibration on Flexible Hoisting System with Time-Varying Length*, Applied Mechanics and Materials, 130-134, pp. 2783-2788, DOI: 10.4028/ www.scientific.net/ AMM.130-134.
19. Vladić, J., Malešev, P., Šostakov, R., Brkljač, N., 2008, *Dynamic analysis of the load lifting mechanisms*, Strojniški Vestnik/Journal of Mechanical Engineering, 54(10), p. 655-661.
20. Li, Z., Qiao, Z., Tang, T., 2011, *Numerical solution of partial differential equations – an introduction to finite difference and finite element methods*, Center for research and scientific comput. & Department of mathematics, North Carolina State University.
21. Vladić, J., Đokić, R., 2017, *Characteristics of mathematical methods and specialized software systems for dynamic analysis of elevators and mining elevators*, IMK-14 - Research and development in Heavy Machinery, 23(2), pp. 31-38.

Contact address:
Radomir Đokić
University of Novi Sad
Faculty of Technical Sciences
21000 Novi Sad
Trg Dositeja Obradovića 6
E-mail: djokic@uns.ac.rs